1

3   Supporting Information for

4 Regional characteristics of variability in the Northern Hemisphere wintertime polar front
5   jet and subtropical jet in observations and CMIP6 models

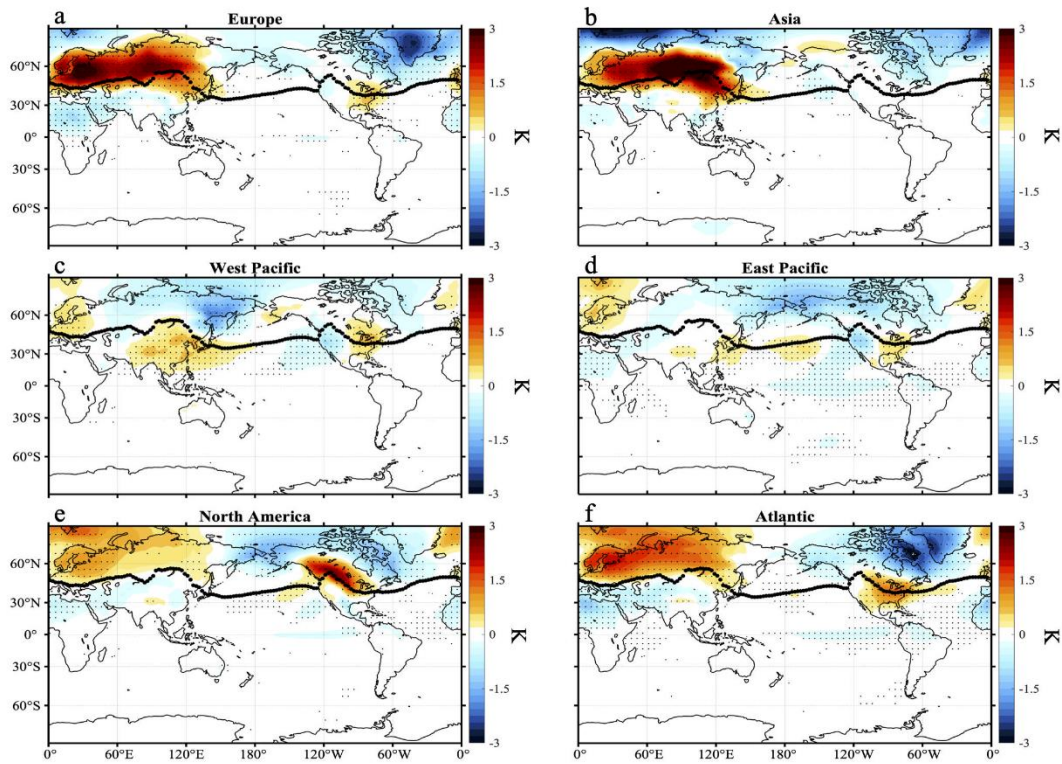6   Xinhuiyu Liu[1], Kevin M. Grise[1], Daniel F. Schmidt[1], Robert E. Davis[1]

7   [1] Department of Environmental Sciences, University of Virginia, Charlottesville, VA, USA

8

9

10 **Contents of this file**

11

14

15

16
17
18
19
20
21
22
23
24
25
26
27
28
29
30
31
32
33

34
35

Regression of surface temperature onto polar front jet position (model-mean)

36
37 **Figure S1.** As in Figure 3, but for the CMIP6 multi-model mean. The regression maps are first
38 calculated individually for each of the 23 CMIP6 models using the wintertime monthly
39 variability of each model over the period 1979–2014, and then these 23 maps are averaged
40 together to form the multi-model mean. Thick black lines on each panel are multi-model-
41 mean climatological PFJ positions. Stippling indicates that more than 80% models agree on
42 the sign of the regression coefficients.

Regression of surface temperature gradient onto polar front jet position (observed)
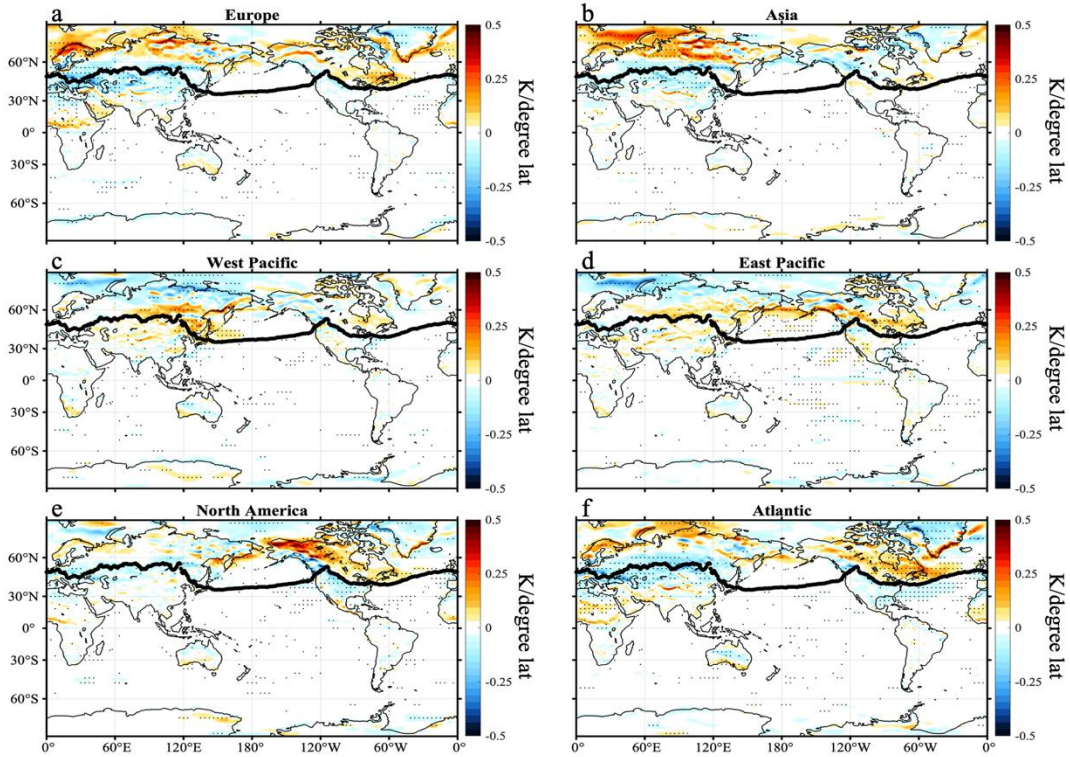
Figure S2. Regression of wintertime monthly surface meridional temperature gradient anomalies onto six different regions' PFJ position in observations. Patterns correspond to surface meridional temperature gradient anomalies (K per degree latitude) associated with a one standard deviation poleward shift of the polar front jet in each region. Surface meridional temperature gradient anomalies are calculated from south to north; therefore, red regions indicate an increase of the meridional temperature gradient. Thick black lines on each panel are climatological PFJ positions in observations as shown in Fig. 1a. Stippling indicates that regression patterns are statistically significant at the 95% level according to a two-tailed Student's t-test.

Regression of surface temperature onto polar front jet strength (model-mean)
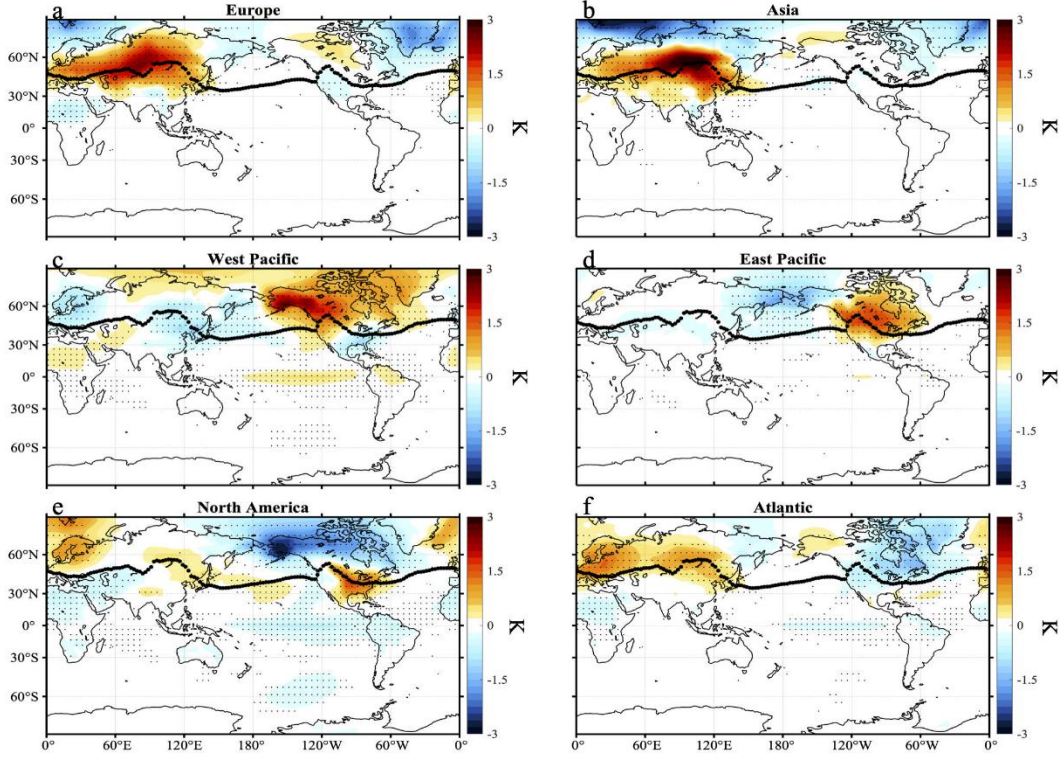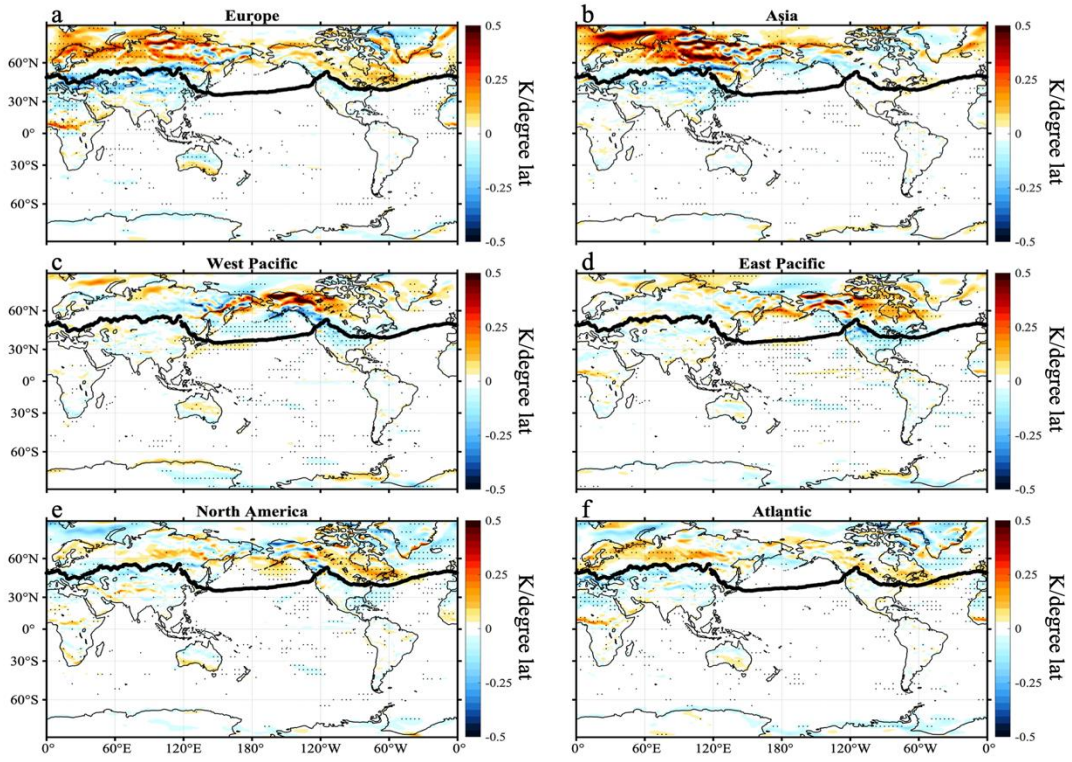

55

Figure S3. As in Figure 4, but for the CMIP6 multi-model mean. The regression maps are first
calculated individually for each of the 23 CMIP6 models using the wintertime monthly
variability of each model over the period 1979–2014, and then these 23 maps are averaged
together to form the multi-model mean. Thick black lines on each panel are multi-model-
mean climatological PFJ positions. Stippling indicates that more than 80% of models agree on
the sign of the regression coefficients.

63

Regression of surface temperature gradient onto polar front jet strength (observed)

64

Figure S4. As in Figure S2, but for the PFJ strength.

Regression of tropical OLR onto polar front jet strength at all longitudes
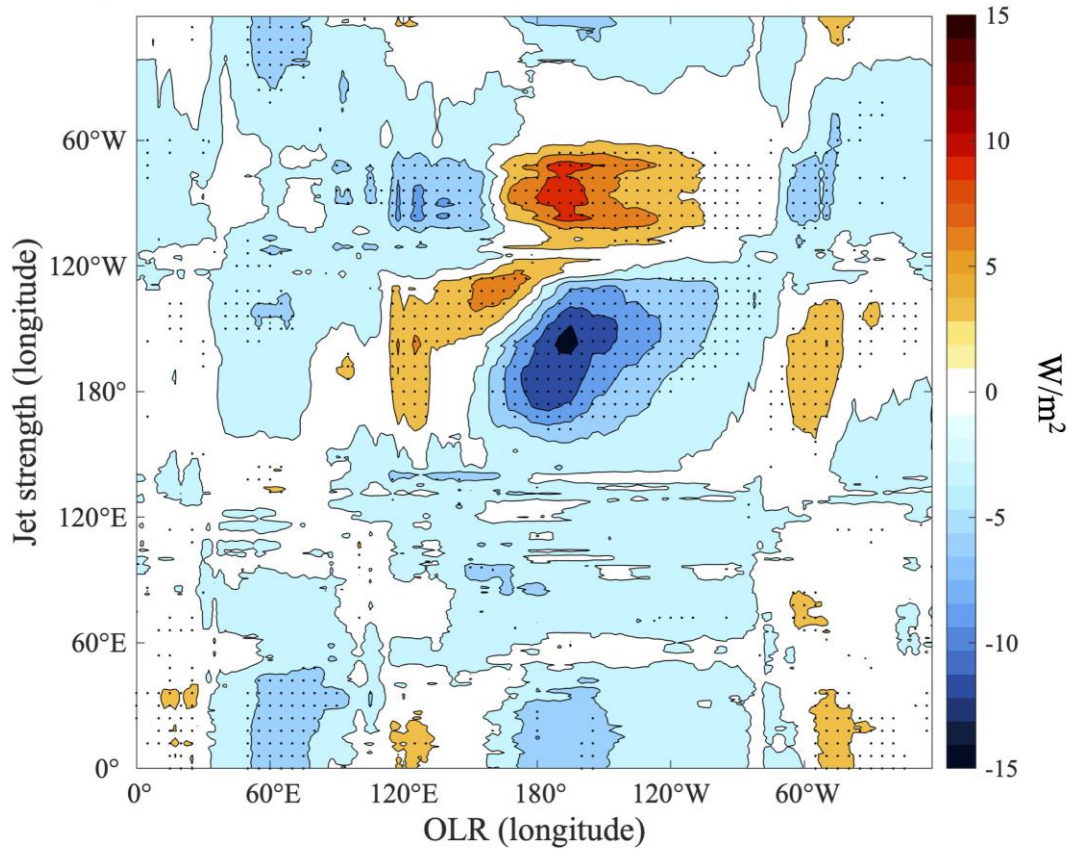
Figure S5. Regression of the tropical OLR (5°S-5°N) anomalies onto polar front jet strength at all longitudes in observations. Color shading represents the regression coefficient of OLR at the longitude on the x-axis to the PFJ strength index at the longitude on y-axis. Stippling indicates that regression patterns are statistically significant at the 95% level according to a two-tailed Student's t-test.
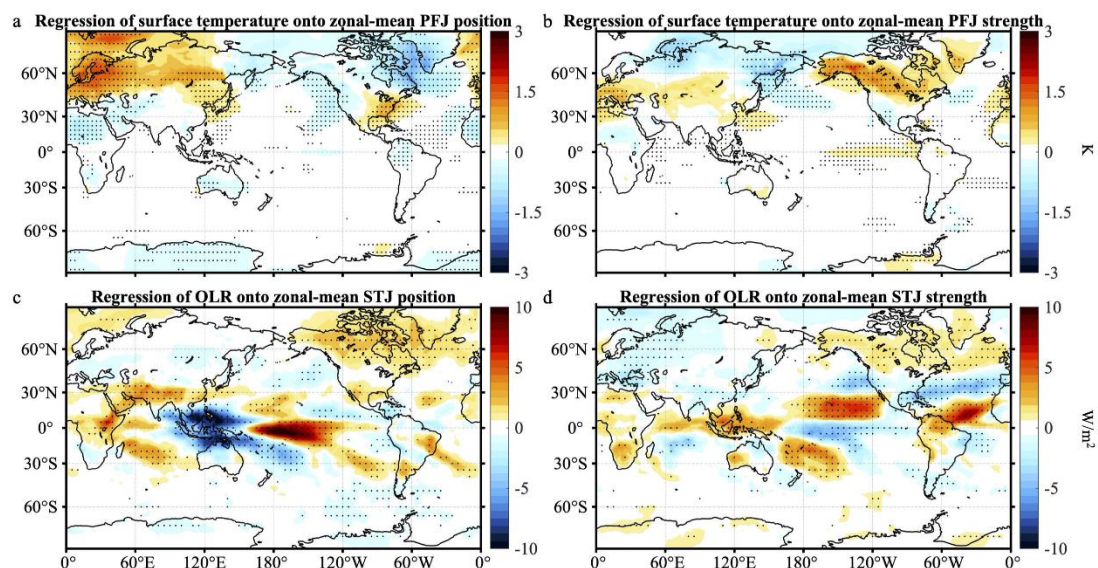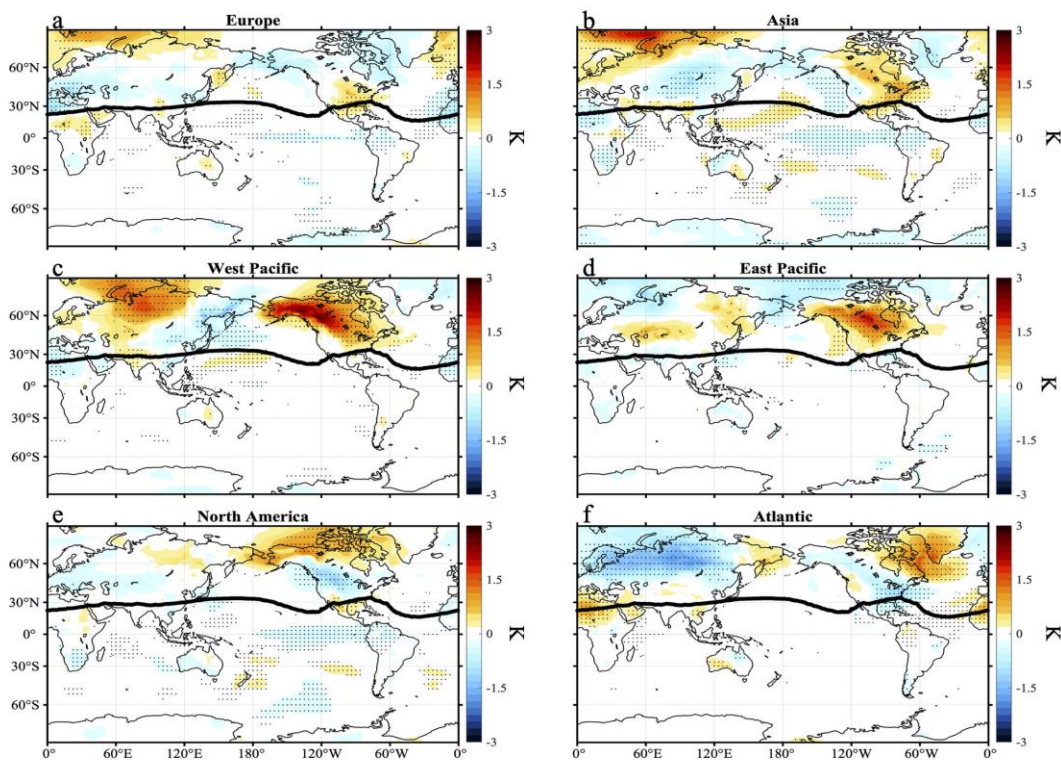
Figure S6. Regression of wintertime monthly surface temperature and OLR anomalies onto zonal-mean jet indices in observations. (a) and (b) are regression coefficients for PFJ position and strength; (c) and (d) are regression coefficients for STJ position and strength. Stippling indicates that regression patterns are statistically significant at the 95% level according to a two-tailed Student's t-test.

103

Regression of surface temperature onto subtropical jet position (observed)

104

Figure S7. As in Figure 3, but for the STJ position.

105

106
107
108

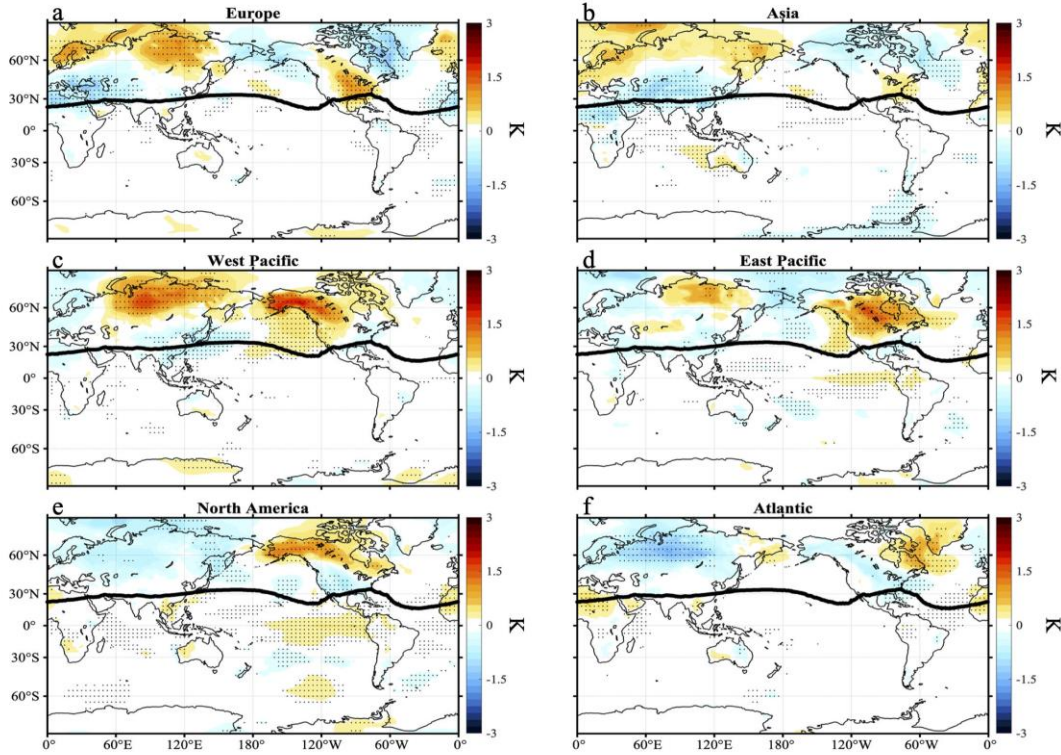Regression of surface temperature onto subtropical jet strength (observed)

109

110 **Figure S8.** As in Figure 4, but for the STJ strength.

111

Regression of OLR onto subtropical jet position (model-mean)

Figure S9. As in Figure 5, but for the CMIP6 multi-model mean. The regression maps are first calculated individually for each of the 23 CMIP6 models using the wintertime monthly variability of each model over the period 1979–2014, and then these 23 maps are averaged together to form the multi-model mean. Thick black lines on each panel are multi-model-mean climatological STJ positions. Stippling indicates that more than 80% of models agree on the sign of the regression coefficients.

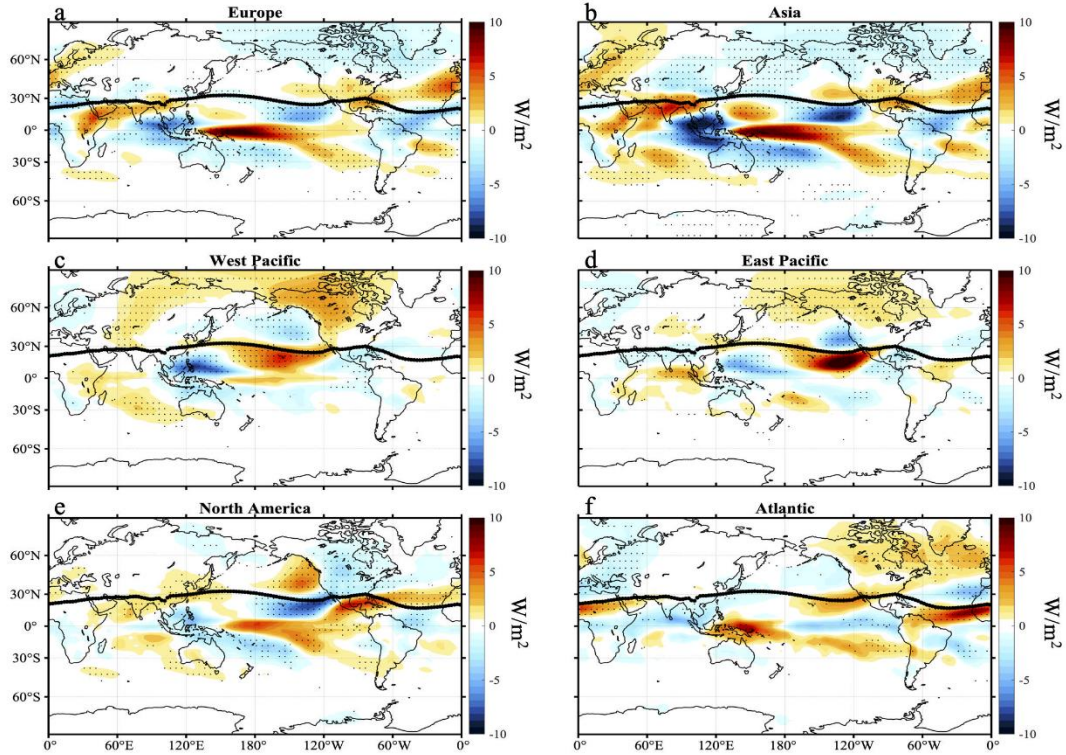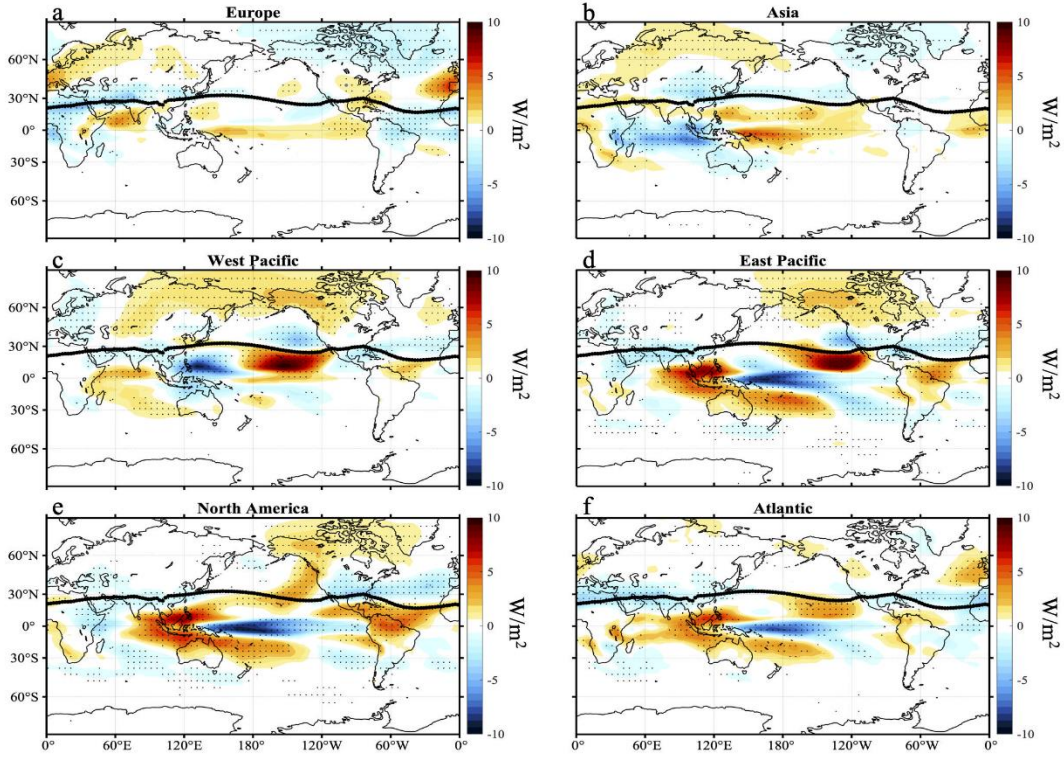## Regression of OLR onto subtropical jet strength (model-mean)

Figure S10. As in Figure 6, but for the CMIP6 multi-model mean. The regression maps are first calculated individually for each of the 23 CMIP6 models using the wintertime monthly variability of each model over the period 1979–2014, and then these 23 maps are averaged together to form the multi-model mean. Thick black lines on each panel are multi-model-mean climatological STJ positions. Stippling indicates that more 80% of models agree on the sign of the regression coefficients.

129

130

Model Number	Model Name	Resolution (latitude x longitude)
	Table S1. Models used in this study	
1	AWI-CM-1-1-MR	0.9375° x 0.9375°
2	BCC-CSM2-MR	1.1250° x 1.1250°
3	BCC-ESM1	2.8125° x 2.8125°
4	CAMS-CSM1-0	1.1250° x 1.1250°
5	CESM2-WACCM	0.9375° x 1.2500°
6	CESM2	0.9375° x 1.2500°
7	CNRM-CM6-1	1.4062° x 1.4062°
8	CNRM-ESM2-1	1.4062° x 1.4062°
9	CanESM5	2.8125° x 2.8125°
10	E3SM-1-0	1.0000° x 1.0000°
11	EC-Earth3-Veg	0.7031° x 0.7031°
12	EC-Earth3	0.7031° x 0.7031°
13	GFDL-ESM4	1.0000° x 1.2500°
14	GISS-E2-1-G	2.0000° x 2.5000°
15	GISS-E2-1-H	2.0000° x 2.5000°
16	HadGEM3-GC31-LL	1.2414° x 1.8750°
17	IPSL-CM6A-LR	1.2587° x 2.5000°
18	MIROC-ES2L	2.8125° x 2.8125°
19	MIROC6	1.4062° x 1.4062°
20	MRI-ESM2-0	1.1250° x 1.1250°
21	NESM3	1.8750° x 1.8750°
22	SAM0-UNICON	0.9375° x 1.2500°
23	UKESM1-0-LL	1.2414° x 1.8750°

132

133 **Table S1.** CMIP6 models used in this study.